Journal: SUBMITTED TO PLOSONE

# A geometric approach to human stress based on stress-related surrogate measures

Petr Kloucek[1], Armin von Gunten[2]

[1] Service of Old-Age Psychiatry, Department of Psychiatry, Lausanne University Hospital, Route de Cery, CH-1008, Lausanne, Switzerland; e-mail: petr.kloucek@iCloud.com

[2] Service of Old-Age Psychiatry, Department of Psychiatry, Lausanne University Hospital, Route de Cery, CH-1008, Lausanne, Switzerland; e-mail: Armin.Von-Gunten@chuv.ch

Keywords: Stress, behavioural complexity, physiological and behavioural surrogate data, self-similar normally distributed processes, non-integer Hausdorff-Besicovitch dimension, Hurst index, behavioural entropy.

## Abstract

We present a predictive Geometric Stress Index (pGSI) and its relation to behavioural Entropy ($b\mathbb{E}$). $b\mathbb{E}$ is a measure of the complexity of an organism's reactivity to stressors yielding patterns based on different behavioural and physiological variables selected as surrogate markers of stress (SMS). We present a relationship between pGSI and $b\mathbb{E}$ in terms of a power law model. This nonlinear relationship describes congruences in complexity derived from analyses of observable and measurable SMS patterns interpreted as stress. The adjective geometric refers to subdivision(s) of the domain derived from two SMS (heart rate variability and steps frequency) with respect to a positive/negative binary perceptron based on a third SMS (blood oxygenation). The presented power law allows for both quantitative and qualitative evaluations of the consequences of stress measured by pGSI. In particular, we show that elevated stress levels in terms of pGSI leads to a decrease of the $b\mathbb{E}$ of the blood oxygenation as a model of SMS.

Corresponding author: Petr Kloucek, petr.kloucek@iCloud.com

## INTRODUCTION

This paper is an extension of our previous spectral theory of human stress, Kloucek and von Gunten (2018), providing a posteriori analysis of stress experienced by a human subject. Here, we explore the possibility to predict mental and physical stress based on a finite number of measurements using various types of artificial intelligence.

Continuous psychological stress monitoring in daily life is important. There are two conventional methods to measure psychological stress, i.e., self-report and body fluid analysis. The self-report method is hard put to monitor human stress consistently due to the lack of standards for stress status. The body fluid analysis is invasive and cannot measure stress continuously.

We intend to illustrate the potential of complexity analytics using physiological and behavioural data of a few normal subjects. More specifically, we decided to use heart frequency variability (HFV) and step frequency (SF) for the analyses as predictor variables of the oxygen saturation in the blood ($SO_2$) as a binary perceptron approximated by peripheral blood oxygenation ($S_pO_2$). These variables will serve as surrogate markers of stress (SMS). We compute the heart frequency variability from HF.

The purpose of this communication is fourfold.

First, we introduce the predictive Geometric Stress Index using HF, SF and $SO_2$. Complexity plays an important role in the objective indexing of SMS patterns Kloucek and von Gunten (2016), Kloucek and von Gunten (2018).

We use the adjective "geometric" to indicate that we compute separation curve(s) in the $(0,1)^2$ complexity space given the complexity projections of HFV $\times$ SF based on the respective values of the perceptron separating normoxemia domain(s) from hypooxemia domain(s).

Second, we re-define $b\mathbb{E}$ we have proposed elsewhere Kloucek, Zakharov, and von Gunten (2016). $b\mathbb{E}$ measures behavioural and/or physiological reactivity distribution of a sequence of different events represented by the complexity of a single pattern corresponding to, e.g., HFV. The concept resides with the assumption that $b\mathbb{E}$ should not be evenly, or nearly so, distributed in time. This

approach is similar to the entropy concept in the physics measuring uneven distributions of energy among atoms. Increasing non-uniform energy distribution increases the entropy of "a non-organic system" while keeping its complexity high. Similar argumentation can be applied to living organisms Schrödinger (1944).

Third, we introduce the predictive Stress Resistance Index (pSRI) that is meant to quantify human resistance to various forms of stress. pSRI is based on perceptron values and their distances to the separation hyperplanes yielded by analyses of time-series of SMS.

Fourth, we propose a power law model linking pGSI with behavioral entropy applying it to time-series of SMS. We strive to predict stress in terms of pGSI in human subjects as measured through the evolution of complexity patterns, using a power law relating pGSI and $b\mathbb{E}(.)$.

In short, we present a proof of concept study showing that complexity analysis of HF and SF and oxygen saturation can be used as SMS to predict human stress.

## METHODS

### *Subjects*

Eight subjects between thirty-five and fifty-five years, four men and four women agreed on carrying a Biovotion's VSM (vital signes monitor) during normal work days including daily routines and sleep.

### *Quantities measured*

- Heart Frequency
  was estimated by means of a motion-compensating algorithm from pulse-induced variations of optical reflection from the skin under the sensor.

- SF
  Movement corresponds to the instantaneous whole-body activity of a human subject. The measurements were performed with a 3-axis accelerometer. The indicator is given by energy

variations of low-passed filtered differentials of accelerometer measurements. SF was determined as the inverse of speed of movement.

- Blood Oxygenation ($SO_2$) was measured using reflected red and infrared light supported by motion-compensating algorithms to estimate the ratio of hemoglobin molecules in arterial blood.

Skin perfusion and temperature were further measures, not used for the purpose of this study.

***Quantities used for the purpose of the study***

We used HFV and SF for the analyses as predictor variables and $SO_2$ as a binary perceptron. The choice of HFV and SF is meant to allow distinguishing increased physical activity (e.g. sport activity leading to congruent increase of HF and SF) from mental stress leading to incongruent HF increase and SF decrease. We felt the limitation to two variables was adequate mainly for two reasons. First, HF (usually its variability) is often used as an indicator of stress, and SF is a reasonable indicator for the intensity of physical activity. Second, we felt the use of only few variables was appropriate for the sake of simplicity for this proof of concept. With the purpose to introduce an element of prediction, we assume that the choice of $SO_2$ as a binary perceptron is adequate. Preliminary analysis revealed that $SO_2$ as measured over time showed a great variability lending itself for the purpose of complexity analyses. Furthermore, the term hypoxemia as used in this paper refers to lower levels of oxygenation relative to the mean oxygen saturation of its complexity. A further reason for the choice of the three SMS is that each of them has much bigger variance over time compared to the rest of the sensory data we had at our disposal (cf. also later).

***Analyses***

We use Logical Regression (LR) Hosmer, Lemeshow, and Sturdivant (2013), Howell (2013), and Artificial Neural Networks (ANN) Kruse (2013), MacKay (2003), Ripley (1996), to obtain separation relative to normoxemia– hypoxemia boundaries in the $H(HFV) \times H(SF)$ complexity

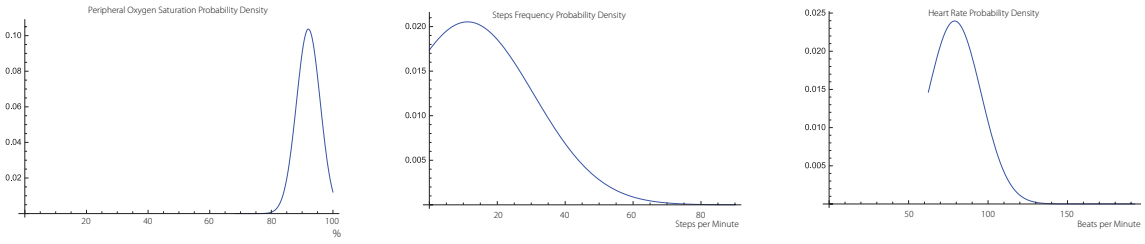


Figure 1. Typical probability densities of the stress indicatrix pertaining to Subject 4. The densities are computed using 1,828 data points representing 54,850 seconds at 30 stroboscopic resolution using histograms based on 60 bins. All three densities are very close to normal distribution and possess approximate self-similarity.

space based on $SO_2$ perceptron binary values. $H(\cdot)$ denotes the Hurst exponent of the enclosed SMS, Mandelbrot and Van Ness (1968). The complexity product space is based on the self-similarity scaling of normally distributed SMS time-series that can be recorded over a meso-temporal time span Mörters and Peres (2010). A typical distribution is shown at Figure 1. Complexity expressed in terms of the Hurst exponent is closely related to the Hausdorff-Besicovitch dimension.

### $SO_2$ *as a Binary Perceptron*

The crucial choice is to select which surrogate data to consider. We choose the HFV complexity and SF complexity as the two $x$ and $y$ axes, which express physiological (HFV) and behavioural (SF) parameters.

We consider the pGSI to depend on three surrogate time discrete processes, i.e. HFV, SF, and $S_pO_2$. The reason for the choice is that each of them have about ten to hundred times bigger variance compared to the rest of the sensory data we measured (cf. Section Variance of Some Sensory Human Data).

Furthermore, we chose SMS with high variance that also had some degree of correlation. Table 4, Table 6 and Table 7 (cf. Annex indicating correlation among HF, SF, and $S_pO_2$). The tables indicate that $SO_2$ is negatively correlated with both HF and SF. The correlation tables also highlight the differences among different subjects.

Subsequently, we chose the complexity of the approximation of $SO_2$ as the third surrogate data, $\mathcal{Z}$. We turn this variable into a binary perceptron using formula (1). The perceptron provides a planar separation, given by smooth curve(s), of H(HFV) and H(SF). We lean on the following argument, tangentially supported by Snyder and Weathers (1977), Nikinmaa (1992), Nikinmaa and Mattsoff (1992), Nikinmaa and Jensen (1992), Chien (1970), leading to the choice of $S_pO_2$ as the binary perceptron.

A further reason for the choice of the $S_pO_2$ as binary perceptron is that stress-hormones-induced changes occur that include the $CO_2/pH$-dependent decrease of the affinity of oxygen to hemoglobin due to the Bohr effect Riggs (1988), thus increasing the oxygenation potential in the tissues.

## RESULTS

### *The Predictive Geometric Stress Index (pGSI)*

We propose a view of some of the acquired SMS leading to the definition of pGSI.

Consider three time-discrete vectors $\mathcal{X} = \{x(t_i)\}_{i=1}^n$, $\mathcal{Y} = \{y(t_i)\}_{i=1}^n$, $n \gg 1$, and $\mathcal{Z} = \{z(t_i)\}_{i=1}^n$ corresponding to three different sets of data representing HFV, SF and $SO_2$. These quantities have different physical units and different ranges. We remove these discrepancies by projecting segmented sub-vectors on the complexity space provided by the Hurst exponent Mandelbrot and Van Ness (1968) or, equivalently, by the Hausdorff-Besicovitch dimension Peitgen, Jügen, and Saupe (1992). Using time equidistant coarse-grained segmentation $\{t_m\}_{m=1}^k$, we compute

$$H : (x(t_m), x(t_{m+1})) \mapsto (0, 1], \qquad \left| \bigcup_{m=1}^{k-1} (t_m, t_{m+1}) \right| = |t_k - t_1|, \quad k > 1. \tag{1}$$

We compute such projections for all three quantities yielding coarse-grained complexity images of the three time-discrete vectors. We denote the new vectors by $H(\mathcal{X})$, $H(\mathcal{Y})$ and $H(\mathcal{Z})$, respectively. We refer to the triple $(H(\mathcal{X}), H(\mathcal{Y}), H(\mathcal{Z})$ as stress indicatrix. This projection, contained in $(0, 1]^3$, is not invertible for we discard micro-structural information contained in the originating time-series.

Further, we construct a binary perceptron $\{\gamma\}_{m=1}^{k}$ mapping $H(\mathcal{Z}) \mapsto \{-1, 1\}$ by

$$\gamma_m \stackrel{\text{def}}{=} \operatorname{sign}\left(H((z(t_m), z(t_{m+1})) - \mathbb{E}\left[H\left(\mathcal{Z}\right)\right]\right), \qquad m = 1, \ldots, k, \tag{2}$$

where $\mathbb{E}[.]$ represents the mean of the enclosed quantity.

Considering the triples $\{H(\mathcal{X})_m, H(\mathcal{Y})_m, \gamma_m\}_{m=1}^{k} \in (0,1)^2 \times \{-1, 1\}$ we solve an optimization problem providing "optimal", possibly closed, curve(s) defining subdomains $\Omega_j^+$ and $\Omega_i^-$, $i, j \in \mathbb{N}$, of $(0,1)^2$ such that $\bigcup_{i>1}\left(\Omega_i^+\right) \cup \bigcup_{j>1}\left(\Omega_j^-\right)$=$(\min(H(\mathrm{HFV})), \max(H(\mathrm{HFV}))) \times (\min(H(\mathrm{SF})), \max(H(\mathrm{SF})))$. The respective subdomains are convex hulls separating points $\{H(\mathcal{X})_m, H(\mathcal{Y})_m\}$ with $\gamma_m = 1$ from the points with $\gamma_m = -1$. The optimization yields the smallest number of these subdomains with the largest area at the expense of allowing a small number of opposite signs to intermix, i.e., some points with $\gamma_m = -1$ can appear in some $\Omega_i^+$. We solve this optimization problem using a combination ANN and LR. The optimization step yields a stress prediction diagram based on the complexity of the acquired SMS using geometric extrapolation that yields planar separation by a $SO_2$ binary perceptron.

Finally, we define pGSI, denoted $\tau$, by

$$\tau\left(H(\mathcal{X}), H(\mathcal{Y}); \gamma\right) \stackrel{\text{def}}{=} \frac{\operatorname{meas}\left(\bigcup_{j\geq 1} \Omega_j^+\right)}{\operatorname{meas}(\Omega)} \in [0, 1]. \tag{3}$$

***pGSI Neutrality Baseline***

We consider $\tau(\cdot, \cdot; \cdot) = \frac{1}{2}$ as the baseline. This approach is justified by the following observation. Let the underlining discrete time-series $\mathcal{X}$, $\mathcal{Y}$ and $\mathcal{Z}$ be normally distributed and self-similar. Then it is plausible to assume that

$$\operatorname{meas}\left(\bigcup_{j>1} \Omega_j^-\right) = \operatorname{meas}\left(\bigcup_{i>1} \Omega_i^+\right) \qquad \text{iff} \qquad \operatorname{card}\left(\{\gamma_j = -1 \mid j > 1\}\right) = \operatorname{card}\left(\{\gamma_j = 1 \mid j > 1\}\right), \tag{4}$$

as $i, j \to +\infty$.

The normality assumptions are true in our computations. Normality distribution accompanied by self-similarity of the chosen surrogate markers for stress is fundamental to characterize the

complexity of SMS. The examples shown in Figure 1 are computed using a histogram map with high resolution bins.

The equality represents the neutral state for it equates distribution of complexities of the surrogate data. The geometry contains more information though. The $HFV \times SF$ complexity space can be divided into four subregions reflecting complexity covariance and contra-variance with respect to higher or lower than expected individual $S_pO_2$, (c.f., Figure 2). The two covariant regions, the lower-left and upper-right quadrants, share the same short/long dynamical memories as well as negative/positive autocorrelation of either complexity of HF and SF time-series. The other two quadrants have opposite characterizations. Consider the upper-left quadrant. While the $x-$axis, representing the complexity of SF, would indicate complex SMS pattern, the HFV axis indicate a more regular pattern. These readings combined with "below-the-mean" personal $SO_2$ can possibly indicate higher physical activity. Furthermore, the lower-right quadrant may indicate mental stress when the complexity of HFV and SF are reversed while the complexity of $SO_2$ is still low.

***Predictive Stress Resistance Index (pSRI)***

The predictive Stress Resistance Index (pRSI) is a further refinement of the pGSI concept. It is based on the idea that the more data points are away from the hypoxemia – nonrmhypoxemia complexity boundary the more resistance to stress a subject will be.

The resistance index, $\theta$, is defined as follows. Let

$$m^+ \stackrel{\text{def}}{=} \text{card}\left(\left\{\left(H(\text{HFV})_j, H(\text{SF})_j\right) \in \bigcup_{i>1} \Omega_i^+\right\}\right). \tag{5}$$

pSRI is then given by, c.f., the left drawing at Figure 5

$$\theta \stackrel{\text{def}}{=} \frac{1}{m^+} \sum_{j=1}^{m^+} \text{dist}\left(\left(\left\{H(\text{HFV})_j, H(\text{SF})_j\right\} \in \bigcup_{i>1} \Omega_i^+\right), \bigcup_{i>1} \partial\Omega_i^-\right). \tag{6}$$

The pGSI is a global index. It can be achieved by uncountably many different configurations of the stress perceptrons. The predictive personalised stress diagram (pPSD) indicates desirable

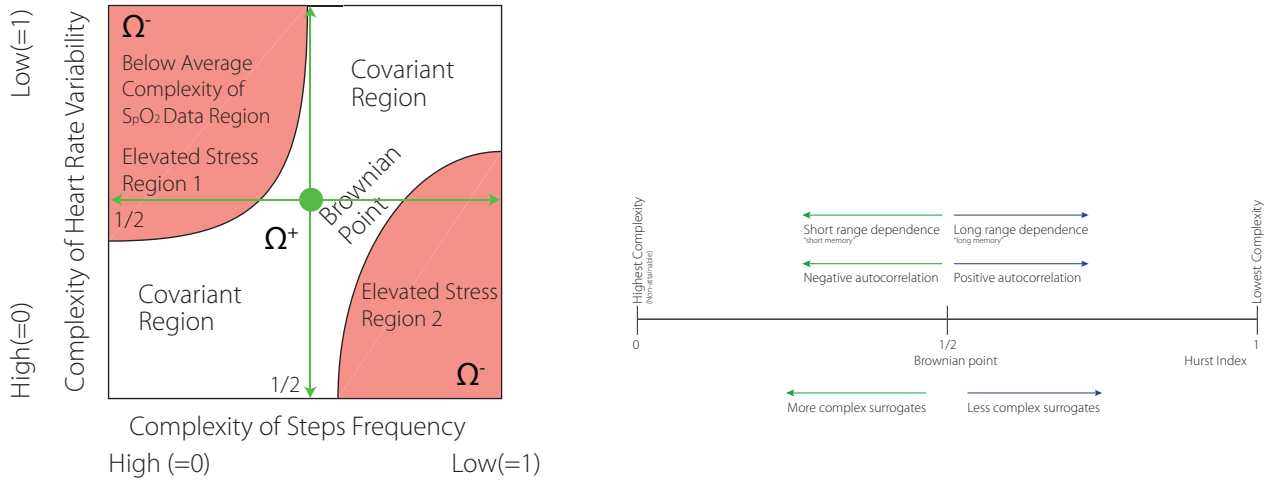


Figure 2. Left: Example of a segmentation of the complexity of HFV × SF space using $SO_2$ as a binary perceptron. $SO_2$ low complexity level, indicating possibly hypoxemia, accompanies incongruent complexity of HFV × SF combinations. Projecting the low levels of $S_pO_2$ onto the HFV × SF two-dimensional space identifies regions with undesirable HFV/SF combinations. Region 1 corresponds to physical stress (high SF): low $SO_2$ complexity, high SF complexity, low HFV complexity, i.e., low $S_pO_2$ relative to individual normhypoxemia. Region 2 corresponds to mental stress: low $S_pO_2$ complexity, low SF complexity, high HFV complexity, i.e., low $S_pO_2$ relative to individual normoxemia despite low motion levels. Right: Interpretation of the complexity indices.

combinations of HRV/SF complexity configurations with respect to a higher level of $SO_2$. The red dots correspond to $\gamma = -1$, the green dots correspond to $\gamma = 1$, i.e., to normoxemia perceptrons.

Comparing pGSI and pRSI for healthy Subject 6 (data are available upon request from authors) we conclude, as an example of the application of the pGSI/pRSI combination, that while pGSI of the Subject 6 ranks fourth, its pRSI is much lower with respect to the control group. This indicates rather medium to low ability to deal with the stress, at least if our assumptions are correct (cf. Figure 6 compared to Figure 7.

### *Entropy of Behavioural Complexity*

Consider a time discrete process $\mathcal{X} = \{X(t_i),\ i = 1, \ldots, m\}$, with its complexity given by the Hurst exponent, $H(X(t_i))$, computed using granulation of an underlying time-series over a uniform

segmentation $(t_i, t_{i+1})$ of $(0, T)$. The Entropy of Behavioural Complexity Kloucek et al. (2016), is defined by

$$b\mathbb{E}(H(\mathcal{X}_m)) \stackrel{\text{def}}{=} \sum_{i=1}^{m} |[\![H(X(t_i))]\!]| \operatorname{sign}(H(X(t_m)) - H(X(t_1))). \tag{7}$$

The Hurst exponent, $H$, denotes the complexity index of acquired normally distributed SMS, $[\![]\!]$ denotes a jump of an enclosed quantity, i.e., $[\![H(\mathcal{X}(t_i))]\!] \stackrel{\text{def}}{=} H(\mathcal{X}(t_i)) - H(\mathcal{X}(t_{i+1}))$, $t_i$ are time equidistant points at which the function $h : t \mapsto H(t)$ has a finite jump. The signum of the difference between the complexities of previous and subsequent states indicate if the behaviours tend to a lower or higher complexity. The negative sign indicates the tendency towards higher complexity, the positive sign indicates the opposite.

We adopt the following localized time discrete notion of the entropy of behavioral complexity (7)

$$b\mathbb{E}(H(\mathcal{X}_m)) \stackrel{\text{def}}{=} \sum_{i=1}^{m-1} |[\![H(X(t_{i+1}))]\!]| \operatorname{sign}(H(X(t_{i+1})) - H(X(t_i))). \tag{8}$$

The above definition of the localized entropy is a sum of signed strengths of the complexity discontinuities.

The definition of $b\mathbb{E}$, (8), accounts also for the history of attaining certain complexity states unlike its definition (7) that accounts only for the sign of the difference between initial and terminal state.

The idea behind the (8) definition is that $b\mathbb{E}$ should be negative if the system evolves, with some probability, to a state with higher complexity and positive when the system evolves towards a lesser complexity state. Let us consider the example presented in Figure ?? using synthetic data generated by normally distributed random numbers. The red piece-wise constant function is represented by $b\mathbb{E} = 2.15$ while the blue, decreasing function, $b\mathbb{E} = -2.95$.

***pGSI relation to $b\mathbb{E}$***

We propose a power law model relating pGSI to respective $b\mathbb{E}(\cdot)$ having the form

$$\alpha\, \mathrm{pGSI}(H(\mathcal{X}), H(\mathcal{Y}); \gamma)^{\beta} \sim b\mathbb{E}(H(\mathcal{V})), \qquad \alpha, \beta \in \mathbb{R}, \tag{9}$$

where $\mathcal{X}$, $\mathcal{Y}$ represent HFV and SF time-series. The third quantity, $\mathcal{Z}$, is represented by $SO_2$ as the binary perceptron $\gamma$ given by (2). The time-series $\mathcal{V}$ represents the remaining quantities.

We identify the power law quantities, $\alpha \in \mathbb{R}$ and $\beta \in \mathbb{R}$, by solving the following non-linear problem

$$(\alpha_j, \beta_j) = \\ \text{Argmin}\left\{\left|a\,\tau\left(H(\mathcal{X}_j), H(\mathcal{Y}_j); \gamma_j\right)^b - b\mathbb{E}(\mathcal{V}_j)\right|^2, \{a, b\} \in \mathbb{R}^2\right\}, j = 1, \ldots, \#\text{ of subjects}, \tag{10}$$

$\tau\left(H(\mathcal{X}), H(\mathcal{Y}); \gamma\right)$ is given by (3).

The different power laws relating pGSI to $bE$ of different patterns might explain the relation between stress and complexity tendencies of SMS time-series. We include the following example as an illustration. Consider $\mathcal{X}$ representing HF, $\mathcal{Y}$ SF complexities and $\mathcal{Z}$ $SO_2$ in the form of its binary perceptron $\gamma$. The computational results indicate, e.g., that

$$0.1\,\tau\left(H(\mathcal{X}), H(\mathcal{Y}); \gamma\right)^{0.6} \approx b\mathbb{E}(H(\mathcal{X})), \tag{11}$$

solving (10).

Scaling laws are shown in Table 2 and visualised by Figure 3.

***Power Laws***

Scaling laws are shown in Table 2 and visualised by Figure 3.

Figure 3 shows $b\mathbb{E}(\cdot)$ of HFV, $SO_2$ and SF as a function of pGSI.

The curves shown at Figure 3 indicate that increased level of stress leads to increased $b\mathbb{E}$ of HFV, Perfusion and Step frequency. The only exception to this is the complexity of $S_pO_2$.

***Correlation of Heart Rate, Steps Frequency and Blood Oxygenation***

We use simple Pearson product-moment correlation coefficient Pearson (1895), to estimate SMS dependency.

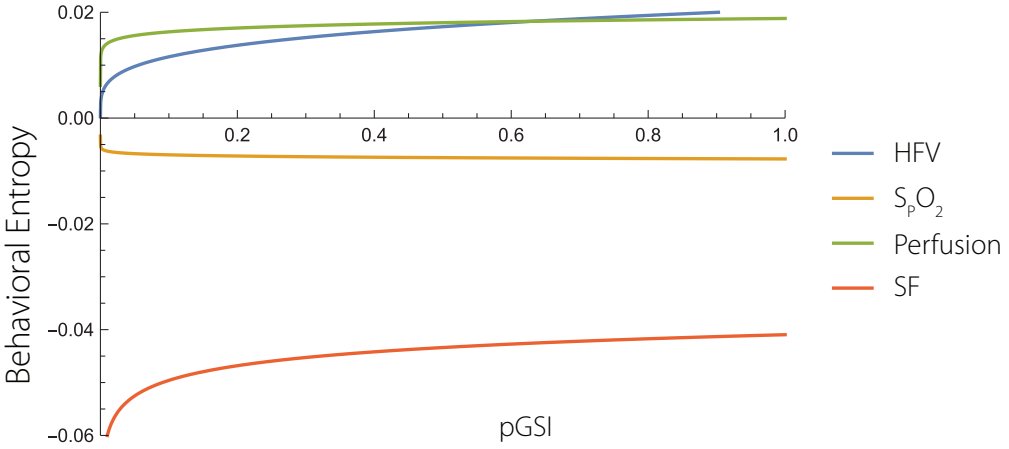


214 Figure 3. $b\mathbb{E}$ power laws. The figure is based on eight healthy subjects. The plot shows how the complexity of different SMS behave
215 with the increasing stress index, pGSI. The curves show that complexity of all SMS increases except for the complexity of the $SO_2$.

221 The data summarised by Table 4, Table 6 and Table 7 show examples of correlations among
222 different sensory quantities of three different subjects. The first two tables correspond to healthy
223 men and women, respectively, the third table corresponds to a female runner, during a typical
224 working day including night/sleep readings. The first two tables show nearly equal negative
225 correlation among $HF/SO_2$, $SF/SO_2$ while that third table indicates positive $HF/S_pO_2$ and nearly
226 none $SF/SO_2$ correlations.

227 ***Mathematical Technicalities***

228 We address in this section some subtle points related to a construction of the personal relative
229 hypoxemia – normoxemia domain partitions in the $H(\mathrm{HFV}) \times H(\mathrm{SF}) \times SO_2$ space, on which we
230 can perform integration in order to compute domains areas to be able to compute pGSI, we can
231 identify domains separation curves, we can compute distances to the separation boundaries, and
232 we can decide which of the acquired SMS belong to which subdomain to be able to compute
233 pSRI.

234 We use both ANN Cain (2017), Schalkoff (1997) and LR Harrell (2001), Everitt (2009), Rossi
235 (2010), Bolstad (2010), in parallel to process the complexity indices of the acquired SMS. The

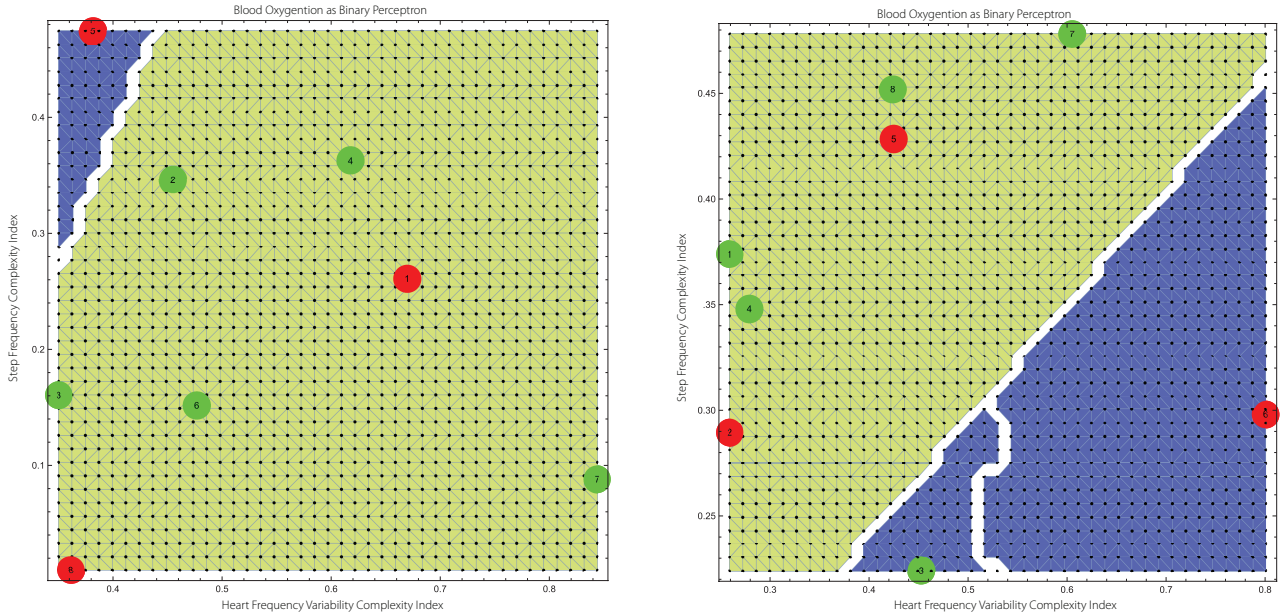


Figure 4. The Delaunay mesh and its separation to normoxemiaand hypoxemia subdomains of Subjects 4 and 6, respectively, used to compute both pGSI and pSRI. The predictive component of the analysis is associated with the assumption that the boundaries $\Gamma_i$, $i = 1, 2$, should remain stable while the complexity data points can move around the effective complexity domain $H(\mathrm{HFV}) \times H(\mathrm{SF})$.

reason we use two different techniques is to deal more effectively with small data sets. In the next step, we apply three different techniques to identify clusters of points forming relative hypoxemia and normoxemia subdomains, i.e., Bray-Curtis Dissimilarity measure/distance (a non-Euclidian distance) Greenacre (2017), Cutsem (1994), Krebs (1999), Chebyschev Distance Cantrell (2000), and Normalized Squared Euclidian Distance. We use Calinski-Harabasz cluster criterion, Caliński and Harabasz (1974). We select then the result with the least number of clusters. We then compute convexification of the respective clusters as a coarse-grained partitioning of the effective domain $H(\mathrm{HFV}) \times H(\mathrm{SF}) \subset (0, 1)^2$. We thus allow some hypoxemia points to belong to normoxemia subdomains and vice-versa. These steps fundamentally simplify subsequent construction of Delaunay triangulations Lee and Schachter (1980), Field (1988), based on the identified points in the complexity effective domain of the respective subdomains. Typically, we use $60 \times 60$ mesh points. Lastly, we disconnect the respective subdomains by small layers improving the quality of the triangulation by avoiding edges of the opposite classification. An example of the outcome of these procedures is shown in Figure 4.

### *Results Pertaining to Human Stress and Stress Resistance*

Below we report a number of findings applying our theory to real individuals. The density plot on the right at Figure 5 shows an example indicating the personal hypoxemia(blue) – normoxemia(yellow) boundary between $H(HFV)$ and $H(SF)$ determined by non-linear optimization using the personal $SO_2$ perceptron.

To interprete the density projection shown in Figure 5, consider two different scenarios. Focusing on the lower boundary of the normoxemia – hypoxemia domain, complexity of HFV,i.e., $H(\text{HFV}) > 1/2$, exhibits lower complexity compared to SF complexity, $H(\text{SF}) < 1/2$, with a ratio of approximately $1:3$. The grey point at this boundary illustrates this scenario. The combination might represent physical activity of a trained and healthy subject.

The second scenario, represented by both $H(\text{HFV})$, $H(\text{SF})$ being below $1/2$, shown by the grey dot at the upper boundary of the $\gamma = 1$ subdomain, indicates that HFV and SF complexities approximately match. Consequently, the first scenario might correspond to a physical stress (high activity), while the second scenario corresponds to a mental stress represented by high complexity of HFV with lower complexity of SF.

Consider segment # 8 (24:00 - 03:00) shown at Figure 5 that corresponds to a period of sleep, in which higher complexity of HFV is accompanied by a near absence of SF complexity and a lower $SO_2$ complexity. Segment # 3 (15:00 - 17:00) is approximately opposite to segment # 8. The segment # 4 has all the characteristics of the first scenario, i.e. physical activity.

### *pGSI and pSRI*

The figure Figure 7 shows comparison between the two measures, pGSI and pSRI. Comparing pGSI and pRSI for Subject 6 we conclude, as an example of the application of pGSI/pRSI combination, that while pGSI of Subject 6 ranks fourth, its pRSI is much lower. According to our interpretation, this may indicate rather medium to low ability to deal with stress (c.f., Figure 6 compared to Figure 7).

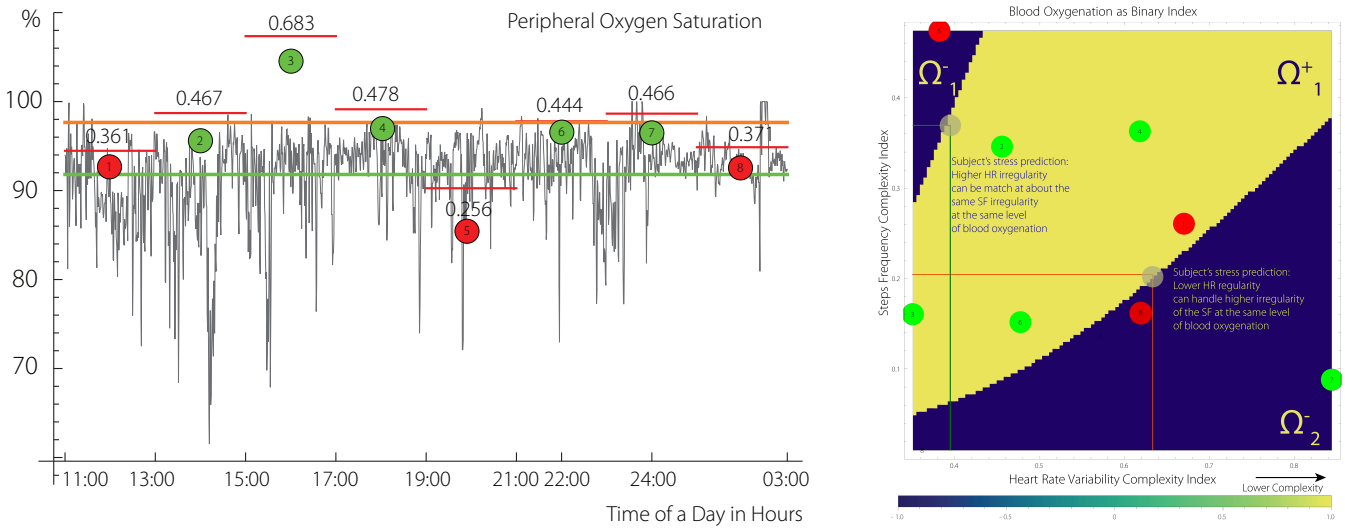


Figure 5. The left plot. Segmentation of $SO_2$ and its projection on $H(HFV)\times H(SF)$ space in the form of $SO_2$ using ANN. The step-like function indicates the value of the Hurst index for each segment. The right plot. The yellow color indicates$SO_2$-perceptron value $\gamma = 1$, given by (2), $\Omega^+$, i.e., normhypoxemia, blue colour indicates $\gamma = -1$, $\Omega_i^-$, $i = 1, 2$. The grey circles are positioned at the boundary of a convex hull of certain number of points with $\gamma = +1$. The analyzed data correspond to a human subject encapsulating 15 hours of SMS acquisition. Each segment contains about 225 data points. The green horizontal line indicates mean of $SO_2$, the orange represents the mean of the complexity segments.

## DISCUSSION

The main idea behind our approach is to use three dimensional phase spaces to model human stress. Our approach is based on the use of $SO_2$ as the binary perceptron as well as HFV and SF as surrogate markers for SMS.

The pGSI index separates high physical activity from what we interpret as mental stress. Our analyses suggests that subjects can be distinguished regarding their overall SMS levels. Our analysis also suggests that stress is not necessarily low during sleep. Both indices, i.e., H(HFV) and H(SF) complexities correspond well with the HF and SF raw data. Low stress modes typically exhibit a positive correlation between HF and $S_pO_2$ while high stress modes have the opposite impact.

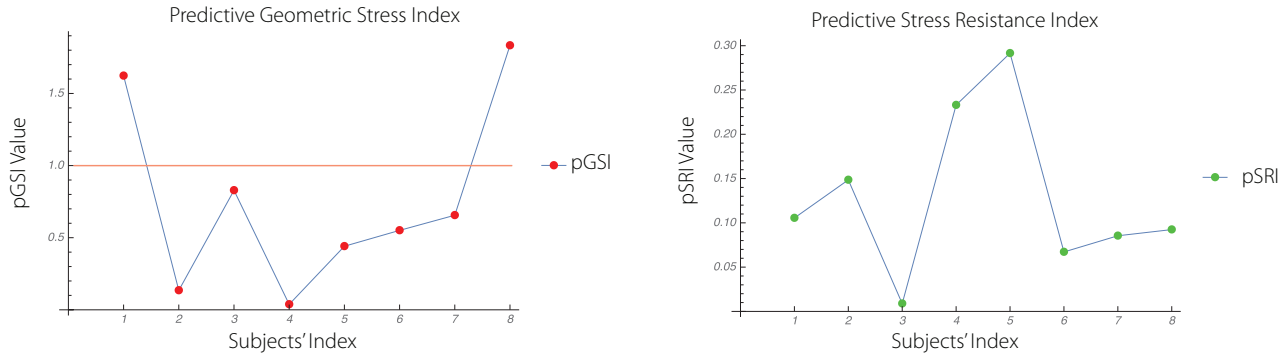


284 Figure 6. pGSIs (left) and pSRIs (right) of eight subjects. The orange horizontal separation line indicates distinction between lower
285 and higher pGSI (c.f. Section pGSI Neutrality Baseline). Comparison of Subjects # 4 and # 5 shows that pGSI and pSRI might be also
286 inversely related.

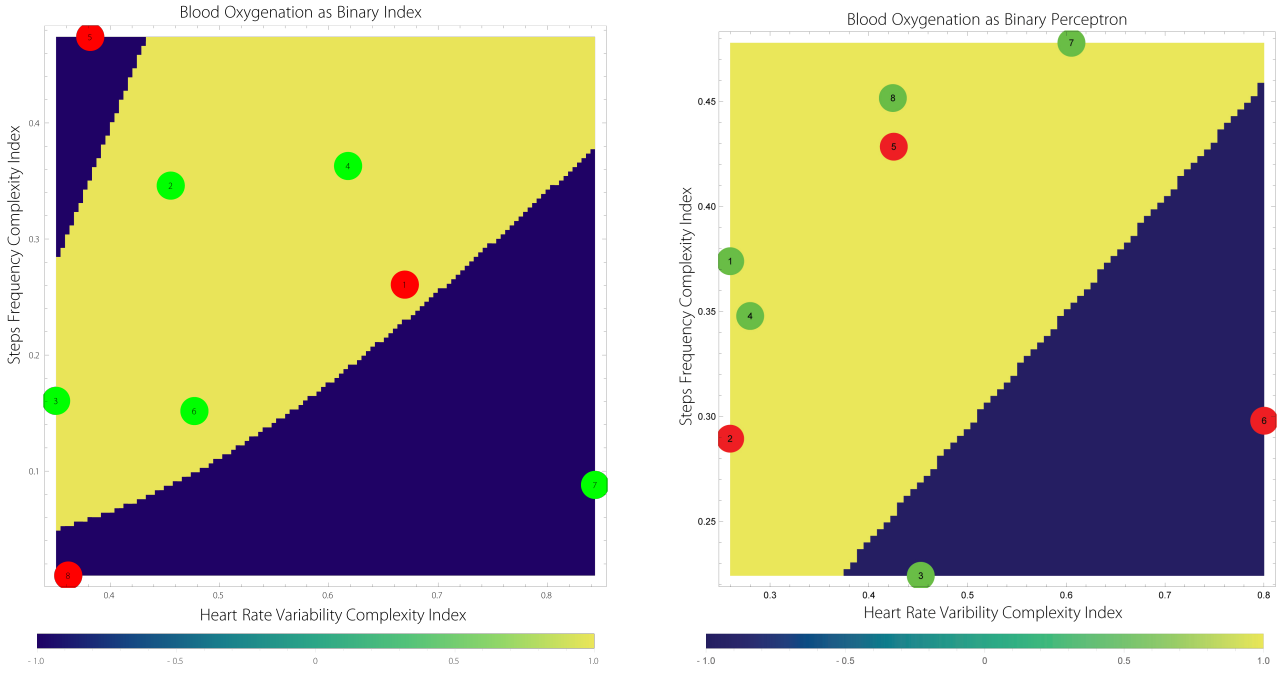


287 Figure 7. The predictive stress diagrams of Subjects 4 (left) and 6 (right) shown are generated using complexity and ANN, LR analyses.

The results obtained using the geometric indices are very similar to those based on spectral theory Kloucek and von Gunten (2018). However, the spectral concept is very different from the geometric one. The combination of HF and SF complexity changes over time predicts $SO_2$ complexity. Based on the variable congruency between HF and SF and the degree of $SO_2$ complexity, behavioural states can be extrapolated (or predicted) as either being in the normal, high-physical activity, or mental stress realm.

For our approach using SMS to achieve clinical relevance we will have to provide evidence of correlation of the results produced by our approach with those obtained through measurements of other indicators of mental stress status. Measuring subjective stress levels or dosing stress hormones in blood or saliva such as $\alpha$-amylase, cortisol or adrenalin, as well as others are necessary to prove clinical usefulness. However, none of the measures just mentioned above can be considered absolute gold standards of stress measurements. Subjective assessment of stress may be hampered in subjects with psychiatric disorders and vary widely among the normal population. Measures of hormones or neurotransmitters in blood or saliva are necessarily coarse-grained over time as they are invasive procedures and constitute no realistic approach in clinical settings. HF variability is sometimes used as another measure of stress and may be considered a gold standard for stress measures. Thus, the relationship between heart rate variability and salivary cortisol levels has been proven (Alberdi et al., 2016). However, the similarity of results of our spectral and geometric approach suggests our approach is promising.

The novelty of the proposed model of stress allows for prediction of building of a stress.

# ANNEXE

| Quantities | HFV | Blood Oxygenation | Perfusion | Skin Temperature | Relative Movement | Steps Frequency |
|---|---|---|---|---|---|---|
| Subject 1 | 0.000187194 | -0.0247733 | 0.0146822 | -0.087012 | -0.214842 | -0.00867333 |
| Subject 2 | 0.00470825 | 0.0169768 | 0.0169838 | -0.00218787 | -0.026098 | -0.0206288 |
| Subject 3 | -0.00816192 | -0.112449 | -0.0693975 | -0.112396 | -0.0567872 | -0.0224971 |
| Subject 4 | -0.0439746 | 0.0014295 | -0.0884581 | -0.0545995 | -0.0105887 | -0.0358108 |
| Subject 5 | 0.07338 | -0.0185053 | 0.184398 | -0.223067 | -0.0205703 | -0.2314 |
| Subject 6 | 0.0235307 | -0.00451071 | 0.0556966 | 0.0344798 | -0.0328561 | 0.0111028 |
| Subject 7 | -0.0017095 | 0.0120759 | 0.0133848 | -0.0466192 | -0.0314652 | -0.0339552 |
| Subject 8 | 0.0906186 | 0.0362499 | 0.0201563 | 0.0450308 | -0.257795 | -0.004041 |

317 Table 1. $b\mathbb{E}$ of 8 subjects. $b\mathbb{E}$ is computed from equidistant time segments of acquired SMS encompassing about 15 hours of data
318 acquisition.

| Behavioral Entropy/Quantities | HFV | Blood Oxygenation | Perfusion | Skin Temperature | Relative Movement | Steps Frequency |
|---|---|---|---|---|---|---|
| $b\mathbb{E}$(HFV) (Amplitude/Exponent) | 0.07/ 0.4 | | | | | |
| $b\mathbb{E}$($SO_2$) (Amplitude/Exponent) | | 0.1/0.1 | | | | |
| $b\mathbb{E}$(Perfusion) (Amplitude/Exponent) | | | -0.0003/5. | | | |
| $b\mathbb{E}$(Skin Temp) (Amplitude/Exponent) | | | | -0.2/-0.3 | | |
| $b\mathbb{E}$(Movement) (Amplitude/Exponent) | | | | | -0.2/-0.3 | |
| $b\mathbb{E}$(SF)(Amplitude/Exponent) | | | | | | -0.2/0.2 |

Table 2. The the power law is estimated using 8 subjects. The $b\mathbb{E}$ is computed from SMS encompassing about 15 hours of data acquisition per subject.

## *Correlation tables*

| Quantities | pGSI | pSRI | CSSI | $b\mathbb{E}(HFV)$ | $b\mathbb{E}(SF)$ | $b\mathbb{E}(S_pO_2)$ | FRI |
|---|---|---|---|---|---|---|---|
| Subject 1 | 1.44898 | 0.118618 | 5.08567 | -0.094372 | -0.214842 | -0.463229 | 5.08567 |
| Subject 2 | 0.0936795 | 0.156836 | 3.65345 | -0.0669521 | -0.203418 | 0.278933 | 13.3114 |
| Subject 3 | 3.90593 | 0.0201643 | 3.83594 | -0.207423 | -0.0567872 | -0.0693975 | 4.49745 |
| Subject 4 | 0.0356675 | 0.224131 | 3.40091 | -0.100361 | -0.596833 | -0.131314 | 4.30004 |
| Subject 5 | 0.485007 | 0.254013 | 4.6757 | -0.308734 | -0.135028 | 0.184398 | 3.46533 |
| Subject 6 | 0.5625 | 0.14543 | 3.95665 | 0.183051 | -0.447905 | 0.113521 | 136.667 |
| Subject 7 | 1.23153 | 0.075056 | 3.1995 | -0.0466192 | -0.0813598 | 0.153274 | 8.24744 |
| Subject 8 | 1.6087 | 0.11549 | 7.32154 | 0.0450308 | -0.36093 | 0.0201563 | 10.5815 |

Table 3. The complex stress characterization of 8 subjects. The Fatigue Recovery Index, introduced in Kloucek and von Gunten (2016), is abbreviated as FRI. $b\mathbb{E}$ is computed from equidistant two hours time segments of SMS encompassing about 15 hours of healthy human data acquisition. Comparing Subjects 4 and 6, we conclude that lower pGSI is accompanied by higher pSRI, and lower tendency complexities of HFV, SF and $S_pO_2$. The data are corroborated by fatigue recovery in the $Var(\mathrm{HF}) \times H(\mathrm{SF})$ space with the ratio of about $1:30$ in favor of the highly trained Subject 4. Also the posteriori indices, CSSIs, are consistent with the two other indicators. Consider the subject #4: the lowest predictive exposer to stress, second highest resistance to stress, second lowest posteriori stress level during a working day cycle including sleep, second lowest FRI, all the three Behavioral Entropies indicating higher reactivitivness with respect to HFV, SF and $S_pO_2$ Kloucek and von Gunten (2018).

## *Two variance tables*

| Quantities | HFV | Perfusion | Blood Oxygenation | Skin Temperature | Relative Movement | Steps Frequency |
|---|---|---|---|---|---|---|
| HFV | 1 | 0.312616 | -0.40399 | 0.061539 | 0.620625 | 0.591639 |
| Perfusion | | 1 | -0.420654 | 0.0780781 | 0.200189 | 0.322364 |
| Blood Oxygenation | | | 1 | 0.00443487 | -0.366836 | -0.414813 |
| Skin Temperature | | | | 1 | 0.0546847 | 0.0134603 |
| Relative Movement | | | | | 1 | 0.859321 |
| Steps Frequency | | | | | | 1 |

Table 4. The correlation of the SMS for Subject 1. The correlation was obtained from 894 equidistant time segments of acquired data.

| Quantities | HFV | Perfusion | Blood Oxygenation | Skin Temperature | Relative Movement | Steps Frequency |
|---|---|---|---|---|---|---|
| HFV | 1 | -0.0144155 | -0.281479 | -0.178694 | 0.445759 | 0.366347 |
| Perfusion | | 1 | -0.0231772 | -0.090395 | 0.103687 | 0.0946516 |
| Blood Oxygenation | | | 1 | 0.121536 | -0.275235 | -0.268467 |
| Skin Temperature | | | | 1 | -0.337818 | -0.254233 |
| Relative Movement | | | | | 1 | 0.797544 |
| Steps Frequency | | | | | | 1 |

Table 5. The correlation of the SMS for subject 2. The correlation was obtained from 431 equidistant time segments of acquired data.

| Quantities | HFV | Perfusion | Blood Oxygenation | Skin Temperature | Relative Movement | Steps Frequency |
|---|---|---|---|---|---|---|
| HFV | 1 | -0.0304565 | -0.218817 | 0.101863 | 0.468396 | 0.456581 |
| Perfusion | | 1 | -0.0370708 | 0.10752 | 0.123471 | 0.143789 |
| Blood Oxygenation | | | 1 | -0.0848257 | -0.267274 | -0.239368 |
| Skin Temperature | | | | 1 | 0.0983426 | 0.0782243 |
| Relative Movement | | | | | 1 | 0.878678 |
| Steps Frequency | | | | | | 1 |

Table 6. The correlation of the SMS for subject 3. The correlation was obtained from 1160 equidistant time segments.

| Quantities | HFV | Perfusion | Blood Oxygenation | Skin Temperature | Relative Movement | Steps Frequency |
|---|---|---|---|---|---|---|
| HFV | 1 | -0.17864 | 0.251414 | 0.0637194 | 0.625233 | 0.676598 |
| Perfusion | | 1 | -0.413867 | 0.0450275 | 0.124743 | 0.0341549 |
| Blood Oxygenation | | | 1 | -0.0803077 | -0.107687 | -0.0287573 |
| Skin Temperature | | | | 1 | -0.0155391 | 0.0199515 |
| Relative Movement | | | | | 1 | 0.863616 |
| Steps Frequency | | | | | | 1 |

Table 7. The correlation of the SMS for Subject 4. The correlation was obtained from 374 equidistant time segments.

| Quantities | HFV | Perfusion | Blood Oxygenation | Skin Temperature | Relative Movement | Steps Frequency |
|---|---|---|---|---|---|---|
| HFV | 1 | -0.25438 | -0.286885 | -0.303626 | 0.699491 | 0.580695 |
| Perfusion | | 1 | 0.141447 | 0.422901 | -0.044777 | -0.014162 |
| Blood Oxygenation | | | 1 | 0.102708 | -0.148153 | -0.041951 |
| Skin Temperature | | | | 1 | -0.055175 | 0.0165696 |
| Relative Movement | | | | | 1 | 0.905904 |
| Steps Frequency | | | | | | 1 |

334 Table 8. The correlation of the SMS for subject 5. The correlation was obtained from 1826 equidistant time segments.

| Quantities | HFV | Perfusion | Blood Oxygenation | Skin Temperature | Relative Movement | Steps Frequency |
|---|---|---|---|---|---|---|
| HFV | 1 | 0.10924 | -0.129858 | 0.0153075 | 0.350668 | 0.267524 |
| Perfusion | | 1 | -0.146234 | 0.112445 | 0.229024 | 0.206663 |
| Blood Oxygenation | | | 1 | -0.187969 | -0.311809 | -0.207137 |
| Skin Temperature | | | | 1 | -0.0353194 | -0.0188643 |
| Relative Movement | | | | | 1 | 0.778953 |
| Steps Frequency | | | | | | 1 |

335 Table 9. The correlation of the SMS for subject 6. The correlation was obtained from 642 equidistant time segments.

| Quantities | HFV | Perfusion | Blood Oxygenation | Skin Temperature | Relative Movement | Steps Frequency |
|---|---|---|---|---|---|---|
| HFV | 1 | 0.167969 | -0.36686 | -0.0750689 | 0.630799 | 0.608615 |
| Perfusion | | 1 | -0.253866 | 0.200398 | 0.284085 | 0.311865 |
| Blood Oxygenation | | | 1 | 0.217739 | -0.437872 | -0.389442 |
| Skin Temperature | | | | 1 | -0.0674336 | -0.00604729 |
| Relative Movement | | | | | 1 | 0.93125 |
| Steps Frequency | | | | | | 1 |

336 Table 10. The correlation of the SMS for subject 7. The correlation was obtained from 1658 equidistant time segments.

| Quantities | HFV | Perfusion | Blood Oxygenation | Skin Temperature | Relative Movement | Steps Frequency |
|---|---|---|---|---|---|---|
| HFV | 1 | -0.0450726 | -0.112492 | -0.107827 | 0.483597 | 0.479533 |
| Perfusion | | 1 | -0.107982 | -0.0231544 | -0.0138105 | -0.0816 |
| Blood Oxygenation | | | 1 | 0.130734 | -0.236126 | -0.170944 |
| Skin Temperature | | | | 1 | -0.0825037 | -0.032942 |
| Relative Movement | | | | | 1 | 0.901963 |
| Steps Frequency | | | | | | 1 |

337 Table 11. The correlation of the SMS for subject 8. The correlation was obtained from 452 equidistant time segments.

| Quantities | Segment 1 | Segment 2 | Segment 3 | Segment 4 | Segment 5 | Segment 6 | Segment 7 | Segment 8 |
|---|---|---|---|---|---|---|---|---|
| HFV | 22.3652 | 37.8688 | 43.3020 | 70.4190 | 66.9771 | 20.2466 | 27.4566 | 27.9333 |
| Perfusion | 0.00210023 | 0.00303487 | 0.0142073 | 0.00308452 | 0.00448286 | 0.00580235 | 0.0437197 | 0.00561481 |
| Blood Oxygenation | 16.4855 | 44.9826 | 34.3267 | 12.5918 | 12.6589 | 19.9398 | 7.82296 | 4.68279 |
| Skin Temperature | 0.915423 | 0.0705794 | 0.018323 | 0.0235593 | 0.0229517 | 0.0999276 | 0.377792 | 0.27331 |
| Relative Movement | 0.522469 | 0.51333 | 1.06422 | 3.57759 | 1.56432 | 0.498561 | 0.156739 | 0.0188911 |
| Steps Frequency | 54.9058 | 30.7965 | 102.836 | 613.618 | 333.916 | 22.4165 | 3.5368 | 0.00266509 |

Table 12. The variance of the SMS for Subject 4. The variance was obtained from 374 equidistant time segments of acquired data.

| Quantities | Segment 1 | Segment 2 | Segment 3 | Segment 4 | Segment 5 | Segment 6 | Segment 7 | Segment 8 |
|---|---|---|---|---|---|---|---|---|
| HFV | 339.983 | 101.478 | 118.456 | 146.107 | 522.311 | 34.4726 | 19.3977 | 13.9784 |
| Perfusion | 0.0543121 | 0.0315185 | 0.00918733 | 0.00217061 | 0.0114509 | 0.00109113 | 0.00178169 | 0.0134619 |
| Blood Oxygenation | 66.8304 | 68.556 | 16.1578 | 13.3593 | 12.07 | 2.83156 | 3.41918 | 8.13148 |
| Skin Temperature | 0.425757 | 0.44536 | 0.488427 | 0.197185 | 2.53583 | 0.2535 | 0.350932 | 0.0978087 |
| Relative Movement | 4.34773 | 0.263877 | 3.22692 | 2.39485 | 5.16624 | 0.251206 | 0.31262 | 0.712321 |
| Steps Frequency | 447.909 | 20.6665 | 356.858 | 216.062 | 772.406 | 4.34818 | 10.0686 | 22.1422 |

Table 13. The variance of the SMS for Subject 6. The variance was obtained from 642 equidistant time segments of acquired data encompassing about 15 hours of data acquisition.

## DECLARATIONS

### *Authors' Contributions*

Both authors contributed equally to the presented research.

### *Competing Interests*

Both authors declare that they do not have competing interests.

### *Funding*

The presented research was done without any sort of funding.

### *Ethics*

The investigation was carried under ethics application "Indexation mathématique de mesures physiologiques multiples non-invasives en milieu réel chez des sujets sains", CHUV, Lausanne Switzerland.

In addition each subject signed "Informed Consent" prior to measurements of the data.

The collection and handling of data has been carried out in accordance to EU current regulations, GDPR.

## REFERENCES

William M. Bolstad. Understanding computational Bayesian statistics. Wiley series in computational statistics. Wiley, Hoboken, N.J., 2010. ISBN 9780470046098 (cloth) 0470046090 (cloth).

Gayle Cain. Artificial neural networks : new research. Computer science, technology and applications. Nova Publishers, New York, 2017. ISBN 9781634859646.

T. Caliński and J. Harabasz. A dendrite method for cluster analysis. Communications in Statistics, 3(1):1–27, 1974.

C. D. Cantrell. Modern mathematical methods for physicists and engineers. Cambridge University Press, Cambridge, UK ; New York, 2000. ISBN 0521591805 (hb) 0521598273 (pbk.).

S. Chien. Shear dependence of effective cell volume as a determinant of blood viscosity. Science, 168(3934):977–9, 1970.

Bernard van Cutsem. Classification and dissimilarity analysis. Lecture notes in statistics. Springer-Verlag, New York, 1994. ISBN 0387944001.

Brian Everitt. Multivariable modeling and multivariate analysis for the behavioral sciences. Statistics in the social and behavioral sciences series. CRC Press, Boca Raton, 1st edition, 2009. ISBN 9781439807699 (alk. paper) 1439807698 (alk. paper).

D. A Field. Laplacian smoothing and Delaunay triangulations. Comm. Appl. Num. Methods, 4:709–712, 1988.

Michael Greenacre. Ordination with any dissimilarity measure: a weighted euclidean solution. Ecology, 98(9): 2293–2300, 2017. ISSN 1939-9170.

Frank E. Harrell. Regression modeling strategies : with applications to linear models, logistic regression, and survival analysis. Springer series in statistics. Springer, New York, 2001. ISBN 0387952322 (alk. paper).

David W. Hosmer, Stanley Lemeshow, and Rodney X. Sturdivant. Applied logistic regression. Wiley series in probability and statistics. Wiley, Hoboken, New Jersey, third edition edition, 2013. ISBN 9780470582473 (hardback).

David C. Howell. Statistical methods for psychology. Wadsworth Cengage Learning, Belmont, CA, 8th edition, 2013. ISBN 9781111835484 (hbk.) 1111835489 (hbk.).

P. Kloucek and A. von Gunten. On the possibility of identifying human subjects using behavioural complexity analyses. Quantitative Biology, 4(4):261–269, Dec 2016. ISSN 2095-4697.

P. Kloucek and A. von Gunten. The compound spectral indices of human stress. J. Appl. Math, 9(12):1378–1394, 2018.

P. Kloucek, P. Zakharov, and A. von Gunten. The compound indexing of human self-similar behavioural patterns. J. Applied Mathematics, 7:2212–2228, 2016.

Charles J. Krebs. Ecological methodology. Benjamin/Cummings, Menlo Park, Calif., 2nd edition, 1999. ISBN 0321021738.

Rudolf Kruse. Computational intelligence : a methodological introduction. Texts in computer science. Springer, New York, 1st edition, 2013. ISBN 9781447150121 (hard cover alk. paper).

D. T Lee and B. J Schachter. Two algorithms for construting a Delaunay triangulation. Int. J. Computer Inf. Sci, 9:219–242, 1980.

David J. C. MacKay. Information theory, inference, and learning algorithms. Cambridge University Press, Cambridge, UK ; New York, 2003. ISBN 0521642981.

B. Mandelbrot and J. Van Ness. Fractional brownian motions, fractional noises and applications. SIAM Review, 10 (4):422–437, 1968.

P. Mörters and Y. Peres. Brownian motion. Cambridge Series in Statistical and Probabilistic Mathematics. Cambridge University Press, Cambridge, 2010.

M. Nikinmaa. Membrane transport and control of hemoglobin-oxygen affinity in nucleated erythrocytes. Physiol Rev, 72(2):301–21, 1992.

M. Nikinmaa and F. B. Jensen. Inhibition of adrenergic proton extrusion in rainbow trout red cells by nitrite-induced methaemoglobinaemia. J Comp Physiol B, 162(5):424–9, 1992.

M. Nikinmaa and L. Mattsoff. Effects of oxygen saturation on the $CO_2$ transport properties of lampetra red cells. Respir Physiol, 87(2):219–30, 1992.

K. Pearson. Notes on regression and inheritance in the case of two parents. Proceedings of the Royal Society of London, 58:240–242, 1895.

H-O. Peitgen, H. Jügen, and D. Saupe. Chaos and Fractals. Springer-Verlag, New York, 1992.

A. F. Riggs. The bohr effect. Annu Rev Physiol, 50:181–204, 1988. ISSN 0066-4278 (Print) 0066-4278 (Linking).

Brian D. Ripley. Pattern recognition and neural networks. Cambridge University Press, Cambridge ; New York, 1996. ISBN 0521460867 (hardback).

Richard J. Rossi. Applied biostatistics for the health sciences. John Wiley and Sons, Hoboken, N.J., 2010. ISBN 9780470147641 (cloth) 0470147644 (cloth).

Robert J. Schalkoff. Artificial neural networks. McGraw-Hill series in computer science Artificial intelligence. McGraw-Hill, New York, 1997. ISBN 007057118X.

E. Schrödinger. What is life? Cambridge University Press, 1944.

G. K. Snyder and W. W. Weathers. Hematology, viscosity, and respiratory functions of whole blood of the lesser mouse deer, tragulus javanicus. J Appl Physiol Respir Environ Exerc Physiol, 42(5):673–8, 1977.